Development of Phase Morphologies of Poly(methyl methacrylate)-Polystyrene-Toluene Mixtures in Electric Fields

Ganesh Venugopal† and Sonja Krause*

Department of Chemistry and Polymer Science and Engineering Program, Rensselaer Polytechnic Institute, Troy, New York 12180-3590

Received December 26, 1991; Revised Manuscript Received May 8, 1992

ABSTRACT: The evolution of the phase morphology of polystyrene (PS)-poly(methyl methacrylate) (PMMA) blends during solvent casting from toluene solutions in an electric field was studied. Depending on the sizes of the phases and the electric field strength used, ellipsoidal or columnar structures could be obtained. If the field was removed while a considerable amount of solvent was present, columnar structures broke up into spherical phases via the Rayleigh instability. Partial phase diagrams were constructed for the PMMA-PS-toluene system by experimental determination of tie lines and by theoretical simulation of spinodal curves. Dielectric constants, viscosities, and interfacial tensions (using the pendant drop technique) were measured for some of the coexisting phases. Interfacial tensions calculated using the shapes of deformed drops in electric fields were very low (10^{-5}-10^{-4} dyn/cm), 2-3 orders of magnitude smaller than those measured by the pendant drop method. Possible reasons for this difference are discussed.

Introduction

The properties of an immiscible polymer blend depend on its phase morphology and the adhesion between the phases; the phase morphology depends on the thermodynamics and kinetics of polymer blend formation. In terms of experimental parameters, this translates to a dependence on polymer molecular structures, composition, molecular weights, and the method of blend preparation. The phase morphology most often observed in polymer blends is that in which one phase forms a dispersion in a matrix of the second phase.[1] Processing conditions can often induce changes in morphology. For example, during extrusion or injection molding, spherical phases may deform into prolate ellipsoids and sometimes into fibrils.[2] Blow molding, on the other hand, tends to change spherical phases into platelets or oblate ellipsoids due to biaxial deformation. Another commonly observed morphology is the cocontinuous or bicontinuous network structure, where both phases form an interpenetrating network. No distinct matrix exists in this case.

In a previous publication[3] we reported the use of electric fields to control polymer blend morphology, more specifically the shape and orientation of the dispersed phases. By solvent casting a poly(ethylene oxide) (PEO)-polystyrene (PS) mixture from cyclohexanone in an electric field, blends with oriented PEO minor phases were prepared. Polymer blend films which consisted of (a) spherical minor phases arranged in the form of pearl chains oriented in the direction of the field or (b) deformed ellipsoidal or columnar minor phases oriented in the direction of the field could be produced. In addition, blends made in electric fields showed larger minor phase dimensions than those made outside the field. The type of morphology formed depended on the molecular weight of the polymers used and the strength of the electric field.

In this paper we investigate the formation and evolution of the deformed phase morphologies in atactic poly(methyl methacrylate) (PMMA)-PS blends formed by solvent casting from toluene in an electric field. This blend, unlike the PEO-PS blends investigated earlier,[3] is completely amorphous, thus presenting fewer complications in the investigation.

† Present address: AT&T Bell Laboratories, Murray Hill, NJ 07974.

Experimental Section

Preparation of Polymer Blends. Table I lists the sources and the molecular weight data of all the polymers used in this study. The PS sample was used as received, while the PMMA samples were heated at 90 °C in a vacuum oven for ca. 3 h to remove residual monomer. Solvent casting was done from 4% w:v (weight of polymer:volume of toluene) polymer solutions on glass microscope slides at room temperature. Chromatography grade toluene was used.

Molecular Weight Determination. Polymer molecular weights were determined by gel permeation chromatography (GPC). These measurements were carried out in tetrahydrofuran (THF) on a Waters unit interfaced with an NEC computer in the laboratory of G. E. Wnek, Department of Chemistry, RPI. A single linear column (Ultrastyragel, molecular weight range 2×10^3-4×10^6) was used, and the peaks were detected by a Waters R40 differential refractometer. Molecular weight calibrations were done by using PS and PMMA standards purchased from Scientific Polymer Products.

Phase Diagrams and Phase Properties. One tie line each for the PMMA38-PS220-toluene system and the PMMA88-PS220-toluene system was obtained as follows. In each case, the two polymers were dissolved individually in toluene to form homogeneous solutions. Mixing these two solutions led to a turbid, phase-separated system. The two phases were allowed to separate from each other at room temperature; because of the high viscosities of the two phases, this process took ca. 5 weeks. A small amount of each phase was then removed using a syringe and weighed. The solvent was evaporated from each phase, and the residual polymer was weighed to give the ratio of solvent to total polymer. The polymer phase was then dissolved in $CDCl_3$ for ^1H NMR spectroscopy. The ratios of the two polymers in each phase were calculated by comparing the areas under the PS aromatic peaks and the PMMA ester methyl peaks. The areas were obtained by integrating the NMR spectrum in the regions of interest. These ratios and the total polymer composition were used to calculate the individual polymer composition in each phase. NMR spectroscopy was done on a 200-MHz Varian XL-200 Fourier transform (FT) NMR spectrometer. Tetramethylsilane (TMS) was used as an internal reference. Tie lines with lower solvent compositions were not obtained because the high viscosities of these systems precluded phase separation even after 5 weeks.

After acquiring those few tie lines that could be obtained, it was useful to simulate the spinodal and the critical points, since these allow us to visualize the profile of the whole phase diagram and have insights into the possible phase separation mechanisms. These simulations were done as follows. For the spinodal, a program was written in Advanced Basic for an IBM personal computer. In this program, eq 1, the spinodal condition[4] for a

0024-9297/92/2225-4626$03.00/0

Table I
Molecular Weight Data for Polymers Used

code	polymer	M_w ($\times 10^{-3}$)	M_w/M_n
PS220[a]	polystyrene	217	2.07
PMMA38[b]	poly(methyl methacrylate)	38.7	1.87
PMMA88[a]	poly(methyl methacrylate)	88.2	1.98

[a] Aldrich Chemical Co. [b] Scientific Polymer Products.

three-component polymer–polymer–solvent system, was solved analytically.

$$\sum m_i\phi_i - 2\sum m_i m_j(\chi_i + \chi_j)\phi_i\phi_j + 4m_1m_2m_3(\chi_1\chi_2 + \chi_1\chi_3 + \chi_2\chi_3)\phi_1\phi_2\phi_3 = 0 \quad (1)$$

where

$$\chi_1 = \frac{\chi_{12} + \chi_{13} - \chi_{23}}{2} \quad (2)$$

χ_{12} being the interaction parameter between components 1 and 2 and so on. χ_2 and χ_3 may be obtained by analogous substitution of subscripts. ϕ_i is the volume fraction of the ith component, and m_i is the ratio of the molar volume of the ith polymer to that of the solvent (V_1). Molecular weights and interaction parameters were required as inputs. The interaction parameters required in eq 2 were calculated from the Hildebrand solubility parameters.[5] A value of 100 cm^3 was chosen for V_1,[5] and a value of 298 K was used for T. A reasonable range of interaction parameters, in accordance with those reported in the literature,[6] were tried: 0.40–0.45 for the PMMA–toluene system, 0.34–0.38 for the PS–toluene system, and 0.01–0.04 for the PS–PMMA system. The ones which gave spinodals in good agreement with the tie lines were selected.

Since the critical point lies on the spinodal curve, all compositions on the spinodal curve were tested for the critical point condition.[4]

$$\sum \frac{m_i^2\phi_i}{(1 - 2\chi_i m_i\phi_i)^3} = 0 \quad (3)$$

The composition which matched this condition best was taken as the critical point.

Viscosities and Dielectric Constants of the Coexisting Phases. Samples of coexisting phases for viscosities and dielectric constants were obtained as described for the tie lines. A Brookfield Model DV-II digital viscometer with a couvette and spindle attachment in the laboratory of T. Jordan at the General Electric Corporate Research and Development Center, Schenectady, NY, was used to measure viscosities at room temperature. Approximately 10-mL sample sizes were used for each measurement. Spindle speeds of 30–60 rpm were used, giving shear rates of 5–20 s^{-1}.

Dielectric constants of the phases were calculated from the ratio of the capacitance value of a phase to the capacitance of air. Capacitance values were measured at a frequency of 1 kHz on a GenRad 1689M RLC Digibridge equipped with a Mitutoyo Digimatic liquid cell. The distance between the electrodes was maintained at a constant 0.8 mm, and ca. 3 mL of sample was used for each measurement. These measurements were carried out at room temperature in the laboratory of G. E. Wnek.

Interfacial Tension Measurements. Interfacial tension measurements for the tie line compositions, using the pendant drop method,[7] were carried out in the laboratory of J. T. Koberstein, Institute of Materials Science, University of Connecticut. Measurements were carried out using coexisting phases as follows. A drop of the bottom (dense) phase was suspended in the top (light) phase from the tip of a syringe. The image of the drop was magnified and sent to a screen through a video camera. This video image was digitized and a drop profile extracted from it. A theoretical drop profile, using the Bashforth and Adams equations,[8] was fitted to the experimental profile and the interfacial tension calculated from the best fit. The density measurements that were required to calculate interfacial tensions were done using an Anton Paar digital densitometer and an external cell, DMA602, with a 0.3-mL capacity.

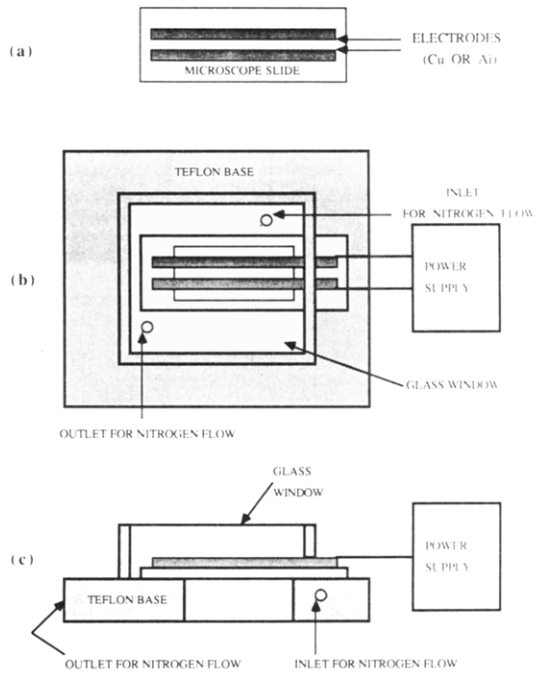

Figure 1. (a) Electrode design used for application of electric field during solvent casting of polymer blends; (b) schematic top view and (c) center cut side view of the microscope stage used for morphology observation during solvent casting in an electric field.

Apparatus for Electric Field Applications. The electrodes (Figure 1a) used to apply electric fields to the samples were made by evaporating either aluminum or copper metal onto glass microscope slides (approximate dimensions = 75 × 25 × 1 mm). Metal evaporation was done using a tungsten basket in a CVC high-vacuum evaporator. Masks made out of 3M scotch tape were used to coat the slides selectively. From the amount of metal used and the distance between the basket and the slide, the electrode thickness was estimated to be 0.1 μm. The gap between the electrodes was usually about 2 mm. The exact distance, when necessary, was measured using a reticle which was attached to the eyepiece of an optical microscope.

Electric fields of up to 20 kV/cm could be applied using a Hewlett-Packard 6516A high-voltage dc power supply. Approximately 5–6 drops of solutions were placed on and between the electrodes. The field was then turned on and the solvent allowed to evaporate. Once all the solvent had evaporated, the field was turned off. To monitor the evolution of polymer blend morphology during solvent casting in an electric field, a Teflon microscope stage (approximate dimensions = 160 × 160 × 10 mm) was designed so that optical microscopy could be performed during the application of the electric field. A top view of this stage is shown in Figure 1b. The slide, with the electrodes on it, was held down by Teflon screws and two metal clips. The clips also acted as contacts between the electrodes and the power supply. The hole in the microscope stage was positioned under the slide. A cover glass window (approximate dimensions = 80 × 80 × 4 mm) covered the slide from the top so that evaporated solvent could be kept away from the objective lens of the microscope. Provision was also made to flow nitrogen gas through the evaporation chamber. A side view of the stage is shown in Figure 1c. This figure is not to scale.

Optical Microscopy. Optical microscopy was done on a Leitz Laborlux 12 Pol S microscope. Morphologies were recorded using either a 35-mm SLR camera or a Polaroid instant camera. A Leitz Auto Photomat attachment allowed accurate determination of exposure times. The objective lens had a magnification of 10× and allowed working distances (distance between microscope slide and objective) of about 8–10 mm. The eyepiece magnification was also 10×.

Results and Discussion

Phase Diagrams and Phase Properties. Tie lines for the PMMA38–PS220–toluene system and the

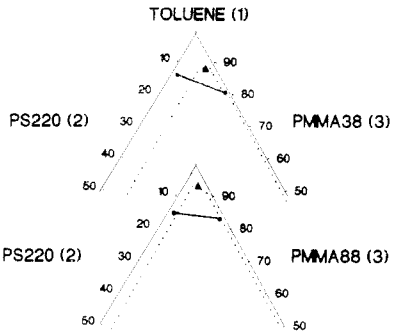

Figure 2. Partial phase diagrams of (a, top) the PMMA38–PS220–toluene system and (b) the PMMA88–PS220–toluene system. Tie line (—), the calculated spinodal curve (···), and the calculated critical point (▲) are shown for each. The interaction parameters used for the calculations were $\chi_{12} = 0.35$, $\chi_{13} = 0.40$, and $\chi_{23} = 0.02$.

Table II
Phase Properties of Demixed PMMA–PS–Toluene Systems

phase	dielectric constant	viscosity (Pa s)	density (g/cm^3)
PMMA38–PS220–Toluene System			
PS rich	2.47	1.17×10^{-1}	0.892
PMMA rich	2.94	0.65×10^{-1}	0.924
PMMA88–PS220–Toluene System			
PS rich	2.49	1.41×10^{-1}	0.893
PMMA rich	2.92	0.51×10^{-1}	0.914

PMMA88–PS220–toluene system were obtained by starting with a 10:10:80 (by weight) PMMA:PS:toluene mixture. The tie lines for both systems, along with the corresponding calculated spinodals and critical points, are plotted in separate phase diagrams in Figure 2. The interaction parameters chosen for the calculations in Figure 2 were $\chi_{12} = 0.35$, $\chi_{13} = 0.40$, and $\chi_{23} = 0.02$, where 1, 2, and 3 stand for toluene, PS, and PMMA, respectively.

The general features of the phase diagram in Figure 2 agree with those obtained by Lau et al.[9] for PMMA–PS–toluene systems with PMMA and PS samples of different molecular weights from the ones used here. As indicated by the interaction parameters, toluene is a better solvent for PS than for PMMA. Hence the PS-rich phase has a higher toluene content than the PMMA-rich phase and is located higher up (in the solvent richer part) of the phase diagram. Therefore the tie line connecting these two points appears tilted.

Table II lists the properties of the phases represented by the tie lines for the PMMA38–PS220–toluene system and the PMMA88–PS220–toluene system. As expected, the dielectric constants of the PMMA-rich phases are larger than those of the PS-rich phases; the dielectric constants of homopolymers PS and PMMA are approximately 2.4 and 3.5, respectively. Also as expected, because of the higher molecular weight of the PS used, the viscosities of the PS-rich phases are greater than the viscosities of the PMMA-rich phases. Since both phases contained mostly toluene and the PS-rich phases contained more toluene than the PMMA-rich phases (see phase diagrams in Figure 2), the densities of the PS-rich phases were lower than those of the PMMA-rich phases.

Evolution of the Morphology of a PMMA–PS Blend in an Electric Field. A sequence of optical micrographs showing the evolution of the morphology of a 50:50 (by weight) PMMA38–PS220 blend from toluene in a 6 kV/cm electric field is shown in Figure 3. In this particular case, liquid–liquid phase separation, as detected by the optical microscope, could be observed starting approximately 19 min after the beginning of the solvent casting procedure. The first (a) and second (b) micrographs (taken 21 and 25 min from the start) show the formation of "whirl pool-like" structures. At this point, due to liquid motion, deformed minor phases were seen moving around rapidly and colliding with other such phases. Very often, some of these phases fused with each other to form larger phases with greater deformation ratios. Phases that were large enough deformed into column-like structures. Some of these columnar structures are visible at the edges of the second (b) micrograph. These structures became more obvious after more solvent was removed (c, d, and e) (taken at 27, 29, and 30 min from the start); by this time the structures had coarsened. This stage was also characterized by a continuous making and breaking of columns. After the 30th min all motion ceased and the morphology was frozen. This final morphology is shown as the sixth micrograph (f).

The swirling motion that was observed while monitoring the morphology evolution during solvent casting (Figure 3) is due to inhomogeneous electric fields in the system, arising from the planar nature of the electrodes that were used. The field is expected to be highest in the plane of the electrode and less above this plane. Liquid motion in inhomogenous fields was also observed by Faraday, who called this motion *rippling*.[10]

Two electric field induced effects were involved in the evolution of the columnar morphology: (1) fusion and (2) deformation. During solvent removal, phase growth and fusion led to larger phases which could deform into ellipsoids (or columns) of larger deformation ratios. The fusion phenomenon occurred after PMMA-rich particles were attracted to each other due to field-induced dielectrophoretic forces,[10] arising from the difference in dielectric constants between the matrix phase and the dispersed phase. Such forces are also known to be the cause for the pearl-chain morphology that was observed in the PEO–PS systems.[3] Furthermore, fusion may also have occurred merely because the solution motion caused two phases to come into contact with each other, a hydrodynamic effect. However, this mechanism of fusion may also be regarded as electric field induced, since the electric field causes this motion. The extent of phase fusion could be decreased by using thicker (1 mm) electrodes. The electric field in the region between these electrodes was more homogeneous than that in the region on and between the thin evaporated electrodes. Hence, the type of morphology formed also depended on the electrode design used and the electric field produced by them.

The deformation of the minor phases was visible as soon as phase separation, as detected by the optical microscope, occurred. At this stage, since the phases were small, the structures that were formed as a result of deformation were ellipsoidal and not columnar. With the systems studied in this work, the electric field strengths at which deformation phenomena were observed were much lower than those that were needed to deform water drops suspended in silicone oil.[11] This may be attributed to the low interfacial tensions that are characteristic of demixed polymer–polymer–solvent systems.[12]

Instability of Columns in the Absence of Electric Fields. In one particular experiment involving the PMMA38–PS220–toluene system (PMMA:PS weight ratio = 20:80), for which micrographs are shown in Figure 4, the field was turned off when the system was fluid and comprised of columnar structures. Rather than collapsing into one big spherical phase, the columns broke up into a number of smaller sized spherical phases. In this case, the field was stepped down from 6 to 0 kV/cm. The

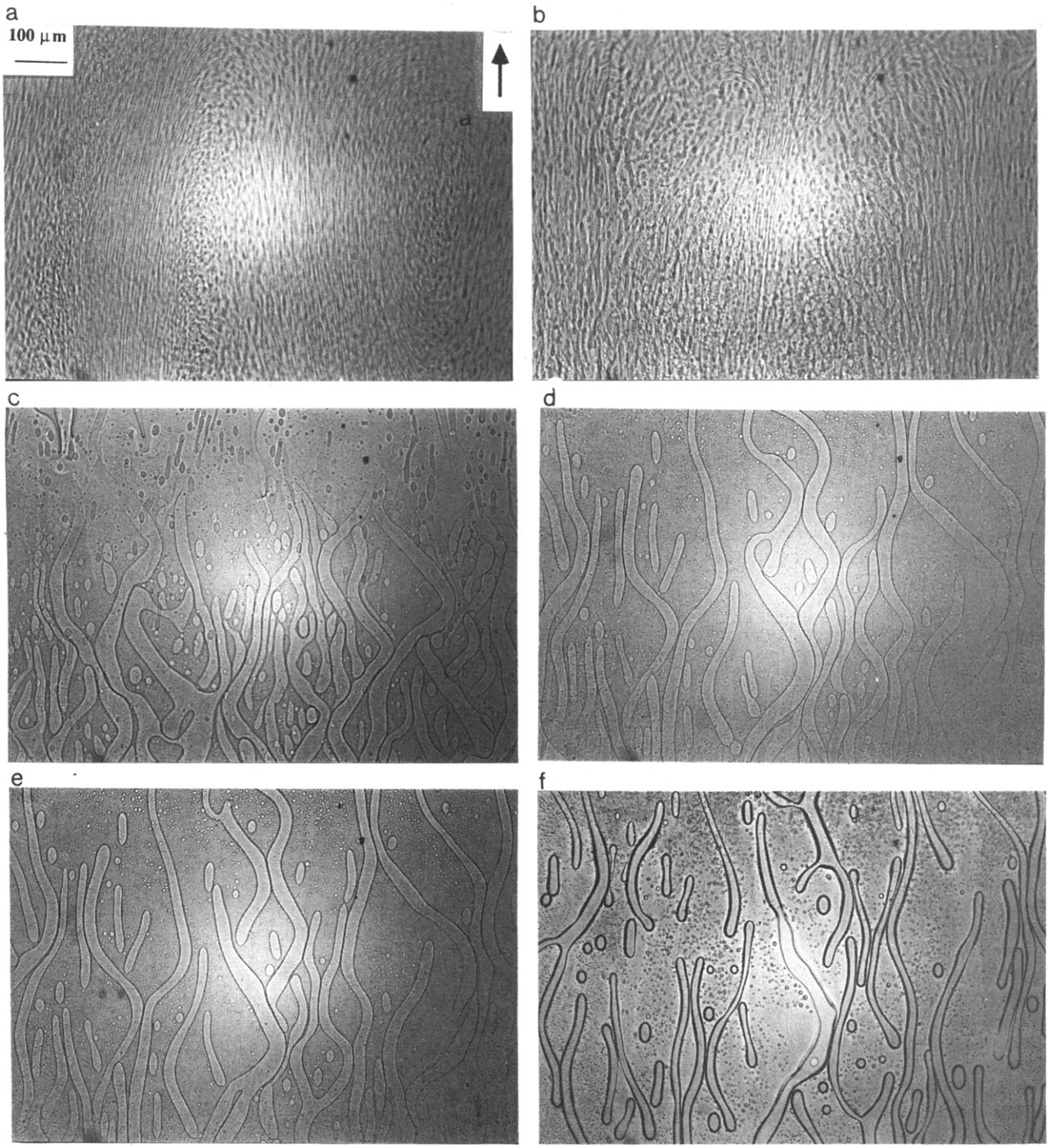

Figure 3. Evolution of the phase morphology of a 50:50 (by weight) PMMA38–PS220 blend, from toluene, in a 6 kV/cm electric field. Approximate times (in minutes) from the start of the solvent casting process were (a) 21, (b) 25, (c) 27, (d) 29, and (e) 30. The final morphology is shown in f. The arrow indicates the electric field direction.

breakdown of the columns into spheres was achieved in approximately 6 s. After breakup into spheres, if the electric field was turned on again, individual spheres deformed into ellipsoids, fusing with neighboring (in the field direction) ellipsoids to form columns in about 3 s.

The breakup phenomenon in fluid cylinders under flow was first observed by Lord Rayleigh and is hence usually referred to as the *Rayleigh instability*. Tomotika[13] was first to study theoretically the instabilities of liquid cylinders in a liquid matrix. According to this theory the rate at which an unstable cylinder breaks up is directly proportional to the interfacial tension and inversely proportional to the radius of the cylinder and the viscosity of the matrix; i.e., thin cylinders surrounded by a low-viscosity matrix and having high interfacial tensions break up fastest. The fact that the columns in the demixed PMMA–PS–toluene system of Figure 4 break up upon removal of the field is caused by the relatively low viscosity (when compared to solvent-free polymer) of the matrix phase due to the presence of solvent (see Table II).

Even if the electric field is not switched off during solvent evaporation, columnar phases may still become unstable and show Rayleigh instability. This may happen if the kinetics of the breakup phenomenon is faster than the time scale of the experiment. Furthermore, as more and more solvent is removed, the interfacial tension is increased.[12,14] Hence, as predicted by Tomotika, the rate of breakup increases during solvent removal. However, the viscosity of both phases increases with solvent evaporation, and this slows down the breakup rate. Since the glass

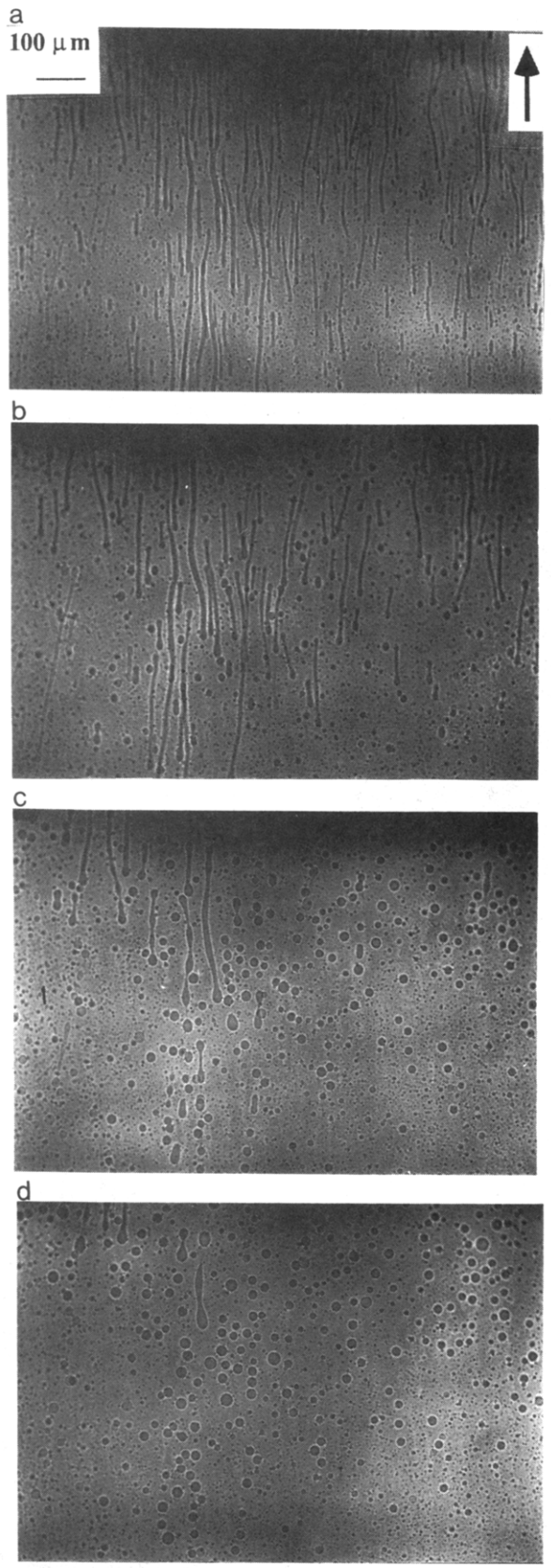

Figure 4. Breakup of PMMA-rich liquid columns upon removal of the electric field. System: PMMA38–PS220–toluene (PMMA:PS weight ratio = 20:80). Micrograph a shows the system in the presence of the electric field. Micrographs b, c, and d show the system 2, 4, and 6 s, respectively, after the electric field was turned off. Arrow indicates electric field direction.

transition temperatures of PS and PMMA are relatively high (~105 °C), the morphology of their blend is expected to freeze at relatively high solvent concentrations, and the system probably solidifies before column breakup becomes rapid. Rayleigh instability in the presence of an electric field has been observed by us in systems which contain poly(vinyl acetate) (T_g ~35 °C) and polystyrene.

Calculation of Interfacial Tensions from Deformation Experiments. The observation that the application of an electric field to a suspension of one phase in another can cause the suspended phase to deform in the direction of the electric field has been made before.[11,15-17] There are two prerequisites for such a process to occur: the first is that the drop be deformable (nonrigid) and the second, that the difference in the dielectric constants of the drop phase (κ_d) and the matrix phase (κ_m) be nonzero. As described by Garton and Krascuki,[11] the strength of the electric field required to bring about such a deformation depends on (1) the magnitude of the difference in dielectric constants, (2) the interfacial tension (σ) between the two phases, and (3) the radius (r) of the suspended phase. The electric field strength, E (in V/cm), required to deform a spherical drop of radius r into a prolate ellipsoid of deformation ratio B (ratio of the major semiaxis to the minor semiaxis of the ellipsoid) can then be given by the equation[11]

$$E = 600\left(\frac{\pi\sigma}{\kappa_m r}\right)^{1/2}\left(\frac{\kappa_m}{\kappa_d - \kappa_m} - G\right)H \tag{4}$$

where G and H are functions of B and are given by

$$G = \frac{1}{B^2 - 1}\left(\frac{B\cosh^{-1}B}{(B^2-1)^{1/2}} - 1\right) \tag{5}$$

and

$$H^2 = 2B^{1/3}(2B - 1 - B^{-2}) \tag{6}$$

The units for σ and r are dyn/cm and cm, respectively; G and H are dimensionless. By letting κ_d/κ_m approach infinity, the case of a conducting droplet in an insulating matrix, eq 4 can be transformed into

$$E = 600\left(\frac{\pi\sigma}{\kappa_m r}\right)^{1/2}GH \tag{7}$$

The quantity GH is known to be a maximum at a B value of around 1.85. When this value is attained by a drop in a system with $\kappa_d/\kappa_m > 20$, the drop is predicted to become unstable and burst.[11] By substituting this value of GH, when $B = 1.85$, into eq 7, the threshold field at which a droplet bursts, E_B, can be estimated as

$$E = 487.7\left(\frac{\sigma}{\kappa_m r}\right)^{1/2} \tag{8}$$

Hence a 0.04-cm water droplet in silicone oil ($\kappa_m = 2$) is expected to burst at 12.3 kV/cm if a σ value of 51 dyn/cm is assumed. Experimentally, a value of 9.5 kV/cm was observed.[11]

It is interesting to note that the system Garton and Krascuki[11] studied showed good agreement with theory despite the fact that the droplet phase in the system, water, invariably contains ionic species that make it slightly conducting. The effect of trace ions and conductivity should be even less in both phases involved in the present study and hence eq 4 is expected to be better suited to this system than the original silicone/water system. Nevertheless, it is important to point out that underestimation of the ratio κ_d/κ_m will lead to values of the calculated interfacial tension that are too low.

Figure 5 shows one particular PMMA phase in a PMMA38–PS220–toluene (PMMA:PS = 20:80) system undergoing progressive deformation with increase in the

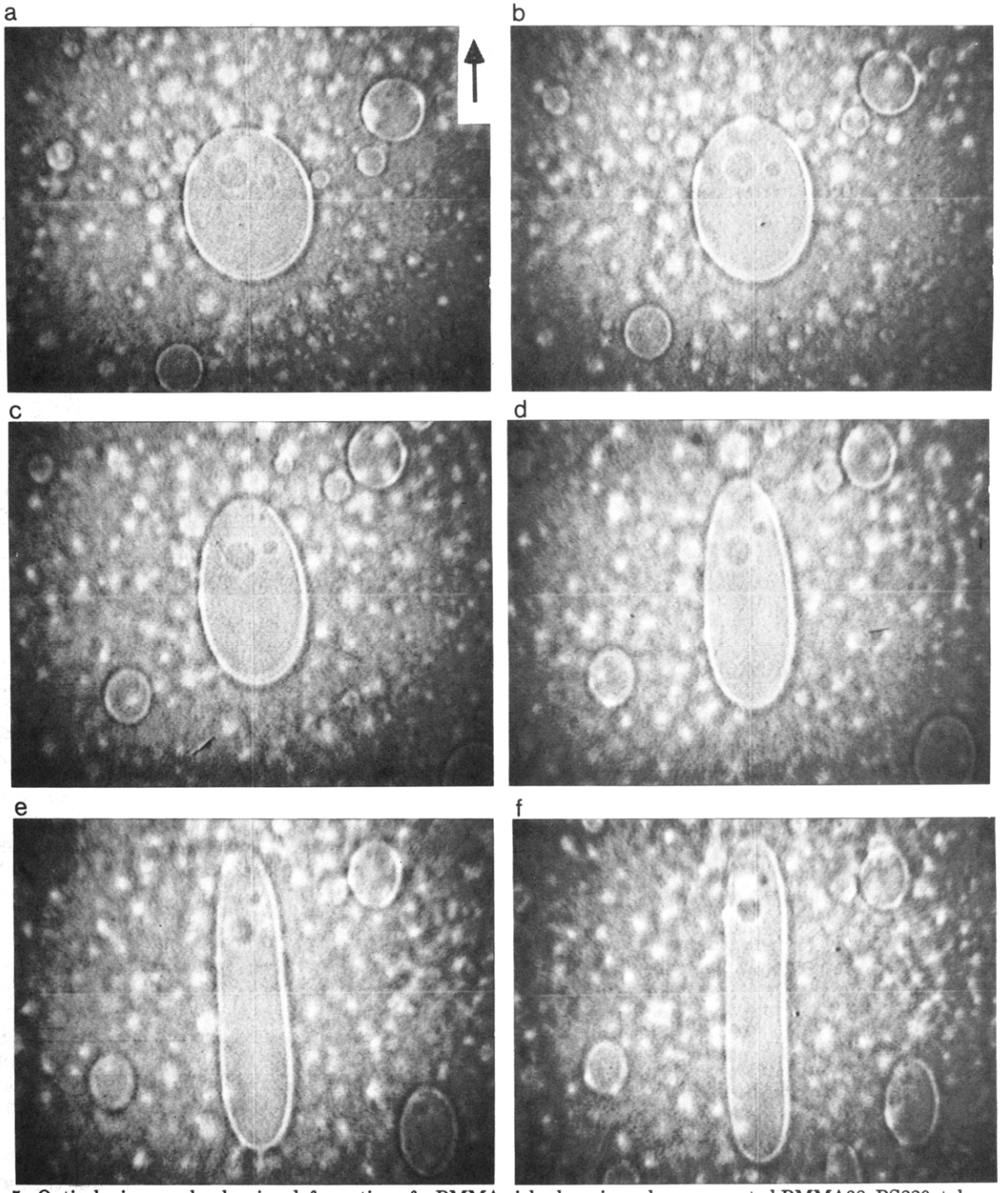

Figure 5. Optical micrographs showing deformation of a PMMA-rich phase in a phase-separated PMMA38–PS220–toluene system (PMMA:PS weight ratio = 20:80) at various fields: (a) 500, (b) 1000, (c) 1500, (d) 2000, (e) 2500, and (f) 3000 V/cm. The undeformed sphere (not shown) is approximately 44 μm in diameter. Arrow indicates electric field direction.

electric field strength from 0.5 to 3 kV/cm. Increasing the field to values higher than 3 kV/cm (the highest in that sequence) led to the fusion of this phase with others and further deformation to form a column-like structure similar to those shown in Figure 3. This increase in deformation ratio with increase in electric field agrees qualitatively with the Garton and Krascuki[11] theory. In addition, no burst behavior was observed in any of the demixed PMMA–PS–toluene systems. This observation is also consistent with a theoretical prediction of Garton and Krascuki[11] since the κ_m/κ_d value of our system could not be greater than 1.5.

The profiles of the drops shown in Figure 5 were used to obtain the interfacial tension between the two phases. The first photograph in the sequence was taken approximately 17 min after the start of the solvent evaporation procedure. The six micrographs were taken within a span of 40 s so that only a negligible amount of solvent evaporated in going from a to f. The total evaporation time was 30 min. This minimization of the time between photographs was essential because the properties of the phases (interfacial tension, viscosity, and dielectric constant) change with the removal of solvent. From Figure 5, values of deformation ratios (B) were measured for the ellipsoids at the different fields. Equation 4, in its cgs units form, was solved for E^2 as a function of σ, as shown in Figure 6 (a plot of E^2 versus the coefficient of σ). The points on the figure were fitted by the method of least squares to a straight line passing through the origin. The slope of this straight line, the interfacial tension, was equal

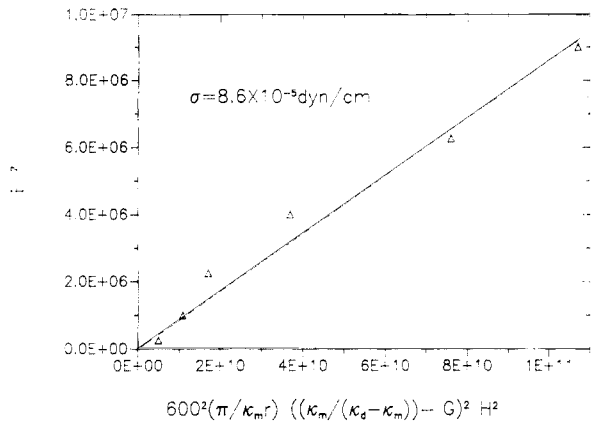

Figure 6. Plot of eq 4 for a single deforming phase in a PMMA38–PS220–toluene system (PMMA:PS weight ratio = 20:80) at various fields (Figure 5). $\kappa_m = 2.47$, $\kappa_d = 2.94$, and $r = 44$ μm. (Δ) Experimental values; (– – –) linear least squares fit forced through the origin.

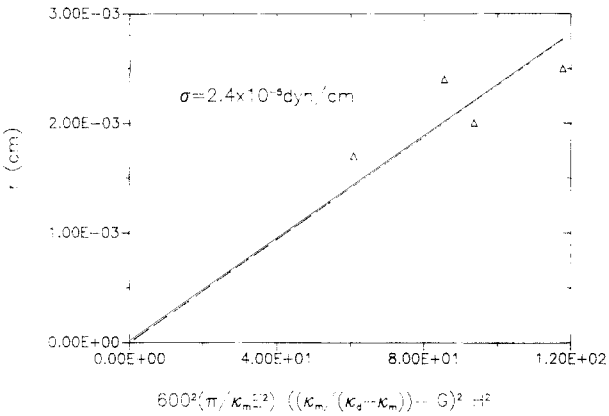

Figure 7. Plot of eq 4 for various-sized deformed phases in a PMMA38–PS220–toluene system (PMMA:PS weight ratio = 50:50) at 1 kV/cm. $\kappa_m = 2.47$ and $\kappa_d = 2.94$. (Δ) Experimental values; (– – –) linear least squares fit forced through the origin.

to 8.6 × 10^{-5} dyn/cm. We call this value of interfacial tension σ_d, the value obtained from deformation measurements.

The PMMA–PS–toluene systems with a PMMA:PS ratio of 50:50 had a larger volume of PMMA-rich phase when compared to the same system with a PMMA:PS ratio of 20:80. As a result, PMMA-rich minor phases in such systems rapidly underwent fusion, and hence a sequence similar to the one in Figure 5 could not be obtained. However, experiments done at fixed electric fields yielded ellipsoidal drop profiles of various size drops, with the larger drops showing larger deformation ratios. Such experiments were done at a field of 1 kV/cm for PMMA38–PS220–toluene (PMMA:PS ratio = 50:50) and at 2.5 kV/cm for PMMA88–PS220–toluene (PMMA:PS ratio = 50:50). To find the interfacial tensions for the 50:50 PMMA:PS systems from these experiments, eq 4 was solved for r as a function of σ. Figures 7 and 8 are plots of r versus the coefficient of σ for the PMMA38–PS220–toluene and the PMMA88–PS220–toluene systems, respectively. The values of r were calculated from the minor (b) and major semiaxes (a) of the ellipsoids using the formula for the radius of a sphere of equal volume: $r = (ab^2)^{1/3}$. The interfacial tension values calculated from these deformation experiments are listed under σ_d in Table III.

The interfacial tension values for the coexisting phases in the demixed PMMA–PS–toluene systems represented by the tie lines in Figure 2 obtained by the pendant drop

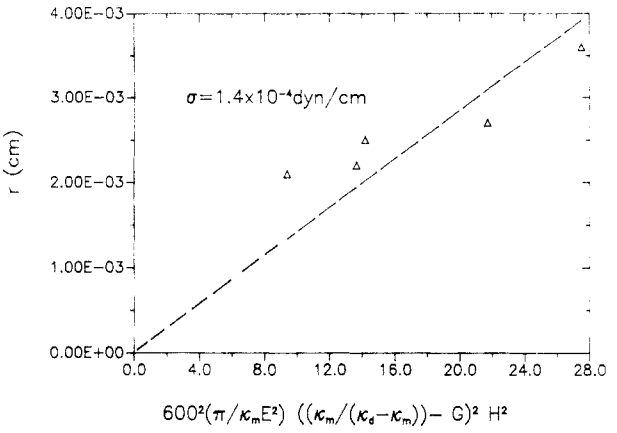

Figure 8. Plot of eq 4 for various-sized deformed phases in a PMMA88–PS220–toluene system (PMMA:PS weight ratio = 50:50) at 2.5 kV/cm. $\kappa_m = 2.49$ and $\kappa_d = 2.92$. (Δ) Experimental values; (– – –) linear least squares fit forced through the origin.

Table III
Comparison of Interfacial Tension Values Obtained from Deformation (σ_d) and Pendant Drop (σ_p) Experiments

system	σ_d (dyn/cm)[a]	σ_p (dyn/cm)[b]
PMMA38–PS220–toluene	2.4 (±0.18) × 10^{-5}	3.9 (±0.16) × 10^{-2}
PMMA88–PS220–toluene	1.4 (±0.13) × 10^{-4}	2.4 (±0.08) × 10^{-2}

[a] The numbers within the parentheses indicate standard errors in the σ_d values obtained from the linear least squares fits in Figures 7 and 8. [b] The numbers within the parentheses indicate standard deviations for the measured σ_p value. Four measurements for the PMMA38 system and three measurements for the PMMA88 system were performed.

method, σ_p, are also reported in Table III. Note that σ_d and σ_p were obtained using starting solutions containing the same ratio of PMMA to PS in each case. This is important because the compositions of the coexisting phases in these mixtures containing polydisperse polymers probably vary with the PMMA to PS ratio in the starting solution.[18] Two important discrepancies are immediately noticeable on comparison of σ_d and σ_p: (1) The σ_d values are in both cases at least 2 orders of magnitude less than the σ_p values; in the PMMA38–PS220–toluene case the two values are different by about 3 orders of magnitude. (2) There is an increase (of an order of magnitude) in σ_d values in going from the PMMA38–PS220–toluene system to the PMMA88–PS220–toluene system, but the σ_p values for the two systems are of the same order of magnitude.

In any case, both the σ_d values and the σ_p values are very low. For comparison, the interfacial tension between n-hexane and water is about 50 dyn/cm[19] and that between PMMA and PS (in the melt form) is around 1 dyn/cm.[20] Low interfacial tensions are necessary for the observation of deformation in the present systems, because otherwise the very small difference in dielectric constants would necessitate the use of much larger fields. Consider a 5-μm droplet with a dielectric constant of 40: if the interfacial tension were around 6 dyn/cm, then even if the dielectric constant of the matrix was only 2, according to eq 4 an electric field of about 50 kV/cm would be required to produce an ellipsoid with a deformation ratio of 2.

Comparison of Interfacial Tensions Obtained by Droplet Deformation and by Direct Measurement. The comparison of σ_d and σ_p values was made on the assumption that the compositions of the coexisting phases represented by the tie lines of Figure 2 are typical of the phases observed in Figure 5 and in the experiments used to determine the data used in Figures 7 and 8. At higher polymer concentrations than were used to obtain these tie

lines, the mixture was so viscous that no further tie lines could be determined. The same high viscosity probably precluded phase deformation in the time scale of our experiments.

The most obvious explanation for the great difference between σ_d and the σ_p is that the two experiments may be measuring σ values in different regions of the phase diagram. During solvent evaporation, the interfacial tension of demixed polymer–polymer–solvent systems is known to increase.[12,14] For example, Langhammer and Nestler[12] found an increase in interfacial tensions as the solvent concentration in a PVAc–chlorinated poly(vinyl chloride)–ethyl oxalate system was reduced. Hong and Noolandi[14] predicted that upon polymerization of the styrene in a polybutadiene–styrene solution the interfacial tension of the phases that separate out increases with increasing extent of polymerization (decreasing amount of styrene monomer). However, our σ_d values were probably measured at compositions poorer in solvent than those shown by tie line I (which is where the σ_p values were obtained) since each deformation experiment was usually carried out in the second half of an approximately 30-min solvent casting period (from the start of the solvent evaporation procedure to freezing of the morphology). This should make σ_d greater than σ_p and is contrary to what was observed. Nevertheless, a more accurate knowledge of the position of the system in the phase diagram during the deformation experiments would be useful. For example, Inoue et al.[21] monitored solvent evaporation in small-angle light scattering experiments by simultaneous measurement of the mass of the system. Such measurements were not possible in the present experiments at this time.

Although all three polymers used in this analysis have unimodal molecular weight distributions, these distributions are fairly broad. This is indicated by the M_w/M_n values in Table I. These broad molecular weight distributions of our polymers may have contributed to the lower interfacial tensions that were calculated using the deformation experiments. Lau et al.[9] observed that the low molecular weight PMMA and PS species in a demixed PMMA–PS–toluene system can migrate into the PS-rich or the PMMA-rich phase, respectively. One may speculate that in the presence of the electric field, a greater migration of the low molecular weight components may take place. If these low molecular weight components reside at the interface rather than in the bulk, this would lower the interfacial tension.

As mentioned earlier, underestimation of the ratio κ_d/κ_m will lead to values of the calculated interfacial tension that are too low. For the PMMA38–PS220–toluene system represented in Figure 7, if we assume an exaggerated κ_d/κ_m value of infinity, we obtain an interfacial tension of 2.5×10^{-2} dyn/cm. This value is in reasonable agreement with the corresponding σ_p (see Table III). However, a similar calculation for the PMMA88–PS220–toluene system (represented by Figure 8) yields an interfacial tension of 1.8×10^{-1} dyn/cm, an order of magnitude different from the corresponding σ_p. This indicates that even though the agreement between σ_d and σ_p may improve by assuming a slightly conductive drop phase, it is unlikely that conductivity is a cause of the discrepancy.

Dependence of Interfacial Tension on Molecular Weight. The deformed drop experiments, which yield σ_d, indicate that there is an increase in interfacial tension of demixed polymer–polymer–solvent systems with increase in the molecular weights of one of the polymers. This increase, by an order of magnitude, could explain the larger fields (by factors of 2–3) that have been necessary to deform the minor phases in the PMMA88–PS220–toluene system when compared to similar-sized phases in the PMMA38–PS220–toluene system.[22] For example, 10% PMMA38–PS220 blends exhibited ellipsoidal morphologies at electric fields as low as 4–5 kV/cm, while 10% PMMA88–PS220 blends showed these morphologies only at fields as high as 12–13 kV/cm. Equation 4 predicts that for an order of magnitude increase in interfacial tension a field that is greater by a factor $10^{1/2}$ (= ~3) has to be applied to see the same extent of deformation.

An increase in interfacial tension with the increase in molecular weights of one of the polymer components has been reported for two-component (polymer–polymer, oligomer–oligomer, and polymer–solvent) systems[23,24] and three-component (polymer–polymer–solvent) systems.[12] For example, Langhammer and Nestler[12] used a capillary rise method to show that interfacial tensions for demixed phases in the system containing PVAc, chlorinated poly(vinyl chloride), and ethyl oxalate increased as the molecular weight of one of the polymers (PVAc) was increased. However, the values of σ_p yielded by the pendant drop method indicate that an increase in molecular weight does not increase the interfacial tension. This result is contrary to the σ_d results and to the literature data on other systems.[12,23,24] Furthermore, since the tie line of the higher molecular weight system is further from the critical point (Figure 2), one would expect a higher σ for this mixture.

If the interfacial tensions are indeed independent of molecular weight, as suggested by the pendant drop (σ_p) measurements, then there is an element lacking in the Garton and Krascuki theory which was used to calculate σ_d when applied to polymeric systems. In that case, we may speculate that the higher electric fields required to observe deformation in the higher molecular weight PMMA–PS220–toluene systems may be a result of the viscoelastic properties of the phases which the theory does not address. Viscosity must play a role in the kinetics of phase deformation, or retraction. For example, Adachi et al.[15-17] calculated the characteristic relaxation time (τ) for the retraction of an ellipsoid to a sphere after removal of an electric field. Equation 9 summarizes this result, where

$$\tau = \frac{(\eta_m + \eta_d)r}{\sigma} \tag{9}$$

η_m and η_d are the viscosities of the matrix and the dispersed phase, respectively. Hence large retraction times should be observed for viscous solutions with low interfacial tensions. Table II indicates that the PMMA-rich phase in the PMMA88–PS220–toluene system has a *lower* viscosity than the corresponding phase in the PMMA38–PS220–toluene system (because, as indicated by the phase diagram in Figure 2, the PMMA88-rich phase has a higher toluene content than the PMMA38-rich phase). Furthermore, the sum of the viscosities of the PMMA-rich and the PS-rich phases for the two systems are almost the same; hence the viscosity contribution to kinetic effects is expected to be the same for both systems. Therefore kinetic arguments based on viscosity alone cannot explain the strong dependence of σ_d values on molecular weights.

Conclusions

The application of an electric field to polymer–polymer–solvent systems during solvent casting produced minor phases with ellipsoidal and columnar morphologies.

(1) By monitoring the morphologies of demixed polystyrene–poly(methyl methacrylate)–toluene systems in an

electric field, it was found that phase fusion and deformation of phases could take place at anytime after the start of the phase separation process.

(2) Larger phases (>100 μm) could be deformed into oriented columnar structures at the field strengths used. These phases broke up into spheres because of the Rayleigh instability when the electric field was removed. The smaller phases (between 10 and 100 μm) formed oriented ellipsoids. Very small phases (<10 μm) only showed deformation in the presence of solvent and appeared spherical in the final morphologies.

(3) Calculation of the interfacial tensions of demixed PMMA–PS–toluene systems from shapes of deformed phases in electric fields yielded very low values (10^{-5}–10^{-4} dyn/cm). However, pendant drop measurements of the same systems yielded interfacial tension values which were higher by 2–3 orders of magnitude.

Acknowledgment. This paper is based upon work partly supported by the National Science Foundation under Grant DMR-9001054. We acknowledge Prof. J. T. Koberstein and Dr. C. Fleischer, Institute of Materials Science, University of Connecticut, for the use of their pendant drop apparatus and Dr. T. Jordan, GE Corporate Research & Development Center, for the use of the viscometer. We are also grateful to Prof. G. E. Wnek for the many fruitful discussions that we have had with him and also for the use of the GPC and the dielectric constant apparatus in his laboratory.

References and Notes

(1) Paul, D. R.; Barlow, J. W.; Keskkula, H. *Encycl. Polym. Sci. Eng.* **1985**, *12*, 399.
(2) White, J. L. In *Polymer Blends and Mixtures*; Walsh, D. J., Higgins, J. S., Maconnachie, A., Eds.; Martinus Nijhoff Publishers: Dordrecht, The Netherlands, 1985.
(3) Venugopal, G.; Krause, S.; Wnek, G. E. *J. Polym. Sci., Polym. Lett. Ed.* **1989**, *27*, 497.
(4) Tompa, H. *Polymer Solutions*; Butterworths: London, 1956.
(5) Krause, S. In *Polymer Blends*; Paul, D. R., Newman, S., Eds.; Academic Press, Inc.: New York, 1978.
(6) (a) Barton, A. F. M. *Handbook of Polymer–Liquid Interaction Parameters and Solubility Parameters*; CRC Press: Boca Raton, FL, 1990. (b) Russell, T. P.; Hjelm, R. P.; Seeger, P. A. *Macromolecules* **1990**, *23*, 890. (c) Lau, W. W. Y.; Burns, C. M.; Huang, R. Y. M. *J. Appl. Polym. Sci.* **1985**, *30*, 1187.
(7) Anastasiadis, S. H.; Chen, J.-K.; Koberstein, J. T.; Siegel, A. F.; Sohn, J. E.; Emerson, J. A. *J. Colloid Interface Sci.* **1987**, *119*, 55.
(8) Ambwani, D. S.; Fort, T., Jr. *Surface Colloid Sci.* **1979**, *11*, 93.
(9) Lau, W. Y.; Burns, C. M.; Huang, R. Y. M. *J. Appl. Polym. Sci.* **1985**, *30*, 1187.
(10) Pohl, H. A. *Dielectrophoresis*; Cambridge University Press: Cambridge, 1978.
(11) Garton, C. G.; Krascuki, Z. *Proc. R. Soc. London, A* **1964**, *280A*, 221.
(12) Langhammer, G.; Nestler, L. *Makromol. Chem.* **1965**, *88*, 179.
(13) Tomotika, S. *Proc. R. Soc. London, A* **1935**, *150*, 322.
(14) Hong, K. M.; Noolandi, J. *Macromolecules* **1981**, *14*, 736.
(15) Moriya, S.; Adachi, K.; Kotaka, T. *Langmuir* **1986**, *2*, 155.
(16) Moriya, S.; Adachi, K.; Kotaka, T. *Langmuir* **1986**, *2*, 161.
(17) Moriya, S.; Adachi, K.; Kotaka, T. *Langmuir* **1988**, *4*, 170.
(18) (a) Koningsveld, R.; Chermin, H. A. G.; Gordon, M. *Proc. R. Soc. London, A* **1970**, *319A*, 331. (b) Kamide, K.; Matsuda, S.; Shirataki, H. *Polym. J.* **1988**, *20*, 949.
(19) *Handbook of Chemistry and Physics*, 70th ed.; CRC Press: Cleveland, 1989.
(20) Anastasiadis, S. H.; Gancarz, I.; Koberstein, J. T. *Macromolecules* **1988**, *21*, 2980.
(21) Inoue, T.; Ougizawa, T.; Yasuda, O.; Miyasaka, K. *Macromolecules* **1985**, *18*, 57.
(22) Venugopal, G. Ph.D. Dissertation Thesis, Rensselaer Polytechnic Institute, Troy, NY, 1991.
(23) LeGrand, D. G.; Gaines, G. L., Jr. *J. Colloid Interface Sci.* **1975**, *50*, 272.
(24) Heinrich, W.; Wolf, B. A. *Polymer*, in press.

Registry No. PS (homopolymer), 9003-53-6; PMMA (homopolymer), 9011-14-7; $PhCH_3$, 108-88-3.